Aalborg Universitet

Fundamental impedance identification method for grid-connected voltage source inverters

Sun, Xiaofeng; Chen , J.; Guerrero, Josep M.; Li, X.; Wang, L.

Fundamental Impedance Identification Method for Grid-Connected Voltage Source Inverters

X. Sun[1], J. Chen[1], Josep M. Guerrero[2], X. Li[1], X. Guo[1]

[1]   College of Electrical Engineering, Yanshan University, Qinhuangdao, 066004, China, e-mail: sxf@ysu.edu.cn, 452253779@qq.com, yddylixin@ysu.edu.cn，guo.x@ysu.edu.cn

[2]   Department of Energy Technology, Aalborg University, Aalborg, DK-9220; Denmark, e-mail: joz@et.aau.dk

Abstract: Considering the importance of line fundamental impedance from the inverter to the point of common coupling (PCC) in microgrids, this study analyzes the influence of fundamental impedance on system stability. Line fundamental impedance values not only apply to decoupled droop control, which can realize accurate control between active and reactive power, but also regulate the droop coefficient to eliminate system circulation, realize power sharing, and improve system stability when a multi-distributed generation system operates in parallel. Moreover, the PCC can sense grid fault on the basis of variations in fundamental impedance. A novel fundamental impedance identification method that adopts a constant power control strategy by varying the active and reactive powers in the grid-connected mode is proposed. In addition, the proposed method has online real-time calculation capability. This strategy has been tested in simulation and in experiments by using a scaled laboratory prototype. Simulation and experiment results verify the accuracy of the proposed scheme.

Keywords: microgrid, identification, fundamental impedance

I.   INTRODUCTION

With the increasing concern on environmental issues and the increasing cost of non-renewable energy sources (RESs), much attention has been given to distributed generation (DG) systems powered by RESs (e.g., solar, wind, and hydraulic power) [1,2,3]. DG systems are connected to the main grid through microgrids, which are energy storage systems and power electronics with "plug and play" characteristics [4,5,6]. The microgrid can operate in both grid-connected and intentional islanding modes, thus enhancing system power reliability. In the grid-connected mode, the microgrid and main grid both provide electric energy to the load. Therefore, the microgrid can independently provide power to the load whenever power quality problems (e.g., voltage sag and power outage) occur in the main grid.

The droop method, which was first developed for parallel uninterruptible power supply systems, controls the active and reactive powers by using frequency and voltage in microgrid by mimicking the parallel operation characteristic of

synchronous generators. The values of the line fundamental resistance and line fundamental inductive reactance are used for the power frame transformation in the decoupling droop control strategy; this strategy can improve system stability and control the power accurately compared with the traditional droop control [7,8,9,10]. The mismatch between line impedances significantly influences reactive power sharing by using the Q–V droop control when multiple DGs operate in parallel in the islanding mode. To eliminate the system circulation caused by line impedance mismatch, a control method is introduced to the interface inverter by using large virtual impedance and by ignoring line fundamental resistance [11–16]. Although this method is easy to implement, virtual impedance may affect the precision of output voltage regulation; thus, a proper virtual impedance value is important for the parallel operation of DG systems to improve the transient and steady-state performance of the systems. Basing on the above analysis, we can denote that line fundamental impedance, together with several modified strategies such as droop control, virtual active and reactive power frame transformation [17,18,19], and adaptive droop coefficients, is crucial for the stable operation of the microgrid.

The point of common coupling (PCC) can sense grid fault on the basis of variations in grid impedance. Grid impedance may be regarded as line impedance from the inverter to the PCC. Therefore, online monitoring of the grid impedance is important to detect unintentional islanding situation of the DGs. For example, an increase in the system impedance can be considered an indication of an islanding scenario. According to the European ENS standard (ENS is the German abbreviation of the main monitoring units with allocated switching devices), an increase of 0.5 W would lead to grid disconnection within 5 s[22]. Thus, several methods have been proposed in the literature to estimate grid impedance[20]–[24]. The following criteria are considered for these methods: accuracy of grid impedance value estimation[22], complexity of the algorithm considering real-time constraints, computational cost of the solution and the required equipment[22], robustness in terms of harmonics and noises, and other real-world constraints. Fast detection should be realized before the current reaches the limiting value (which can lead to the activation of the traditional protective equipment) to avoid power disturbances.

In this study, a fundamental impedance identification method for the grid-connected mode inverter is developed. Fundamental resistance is detected by varying the active power and maintaining the reactive power at zero. Similarly, the fundamental inductive reactance is estimated by varying the reactive power and maintaining the active power at zero. This method is theoretically simple and does not intentionally inject disturbance into the grid, which may lead to power quality degradation issues. The proposed identification method is simple and easy to implement. In addition, real-time and online identification yields accurate result. The proposed control strategy has been tested in simulation and in an experimental platform based on TMS320F2812 DSP. Simulation and experiment results verified the feasibility of the proposed strategy.

II.   MICROGRID STRUCTURE

Figure 1 shows the structure of the microgrid connected to the utility main grid through a static transfer switch at the PCC. DG1 and DG2 are connected to the grid through line impedance. The microgrid and the main grid both provide power under normal operation. Once the microgrid is disconnected from the main grid, the microgrid should be able to supply the total power demand of the loads.
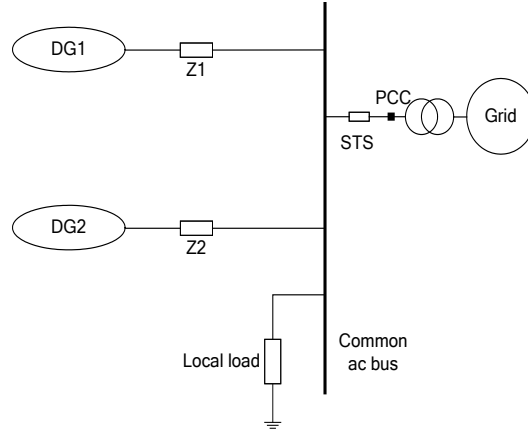

Fig. 1 Microgrid system structure.

Figure 2 shows the equivalent structure of a DG inverter connected to the grid through line impedance. The active and reactive power injected to the grid can be expressed as follows:

$$P = \frac{E_1^2}{Z}\cos\theta - \frac{E_1 E_2}{Z}\cos(\theta + \delta) \tag{1}$$

$$Q = \frac{E_1^2}{Z}\sin\theta - \frac{E_1 E_2}{Z}\sin(\theta + \delta), \tag{2}$$

where E_1 is the common bus voltage, E_2 is the amplitude of the inverter output voltage, δ is the power angle, θ is the impedance angle, and $Z = R + jX$ is the line impedance. Commonly, $\sin\theta = X/Z$ and $\cos\theta = R/Z$. Thus, the following equations can be obtained:

$$E_2 \sin\delta = \frac{XP - RQ}{E_1} \tag{3}$$

$$E_1 - E_2 \cos\delta = \frac{RP + XQ}{E_1}. \tag{4}$$

The power angle δ in Equations (3) and (4) is related not only to the active power but also to the reactive power; thus, the difference in the voltage magnitude is determined by both active and reactive powers. Consequently, the traditional P-f droop control, which ignores the effect of line resistance, may result in active and reactive power

coupling. Therefore, determining the fundamental line resistance and fundamental line reactance are important to ensure system stability.
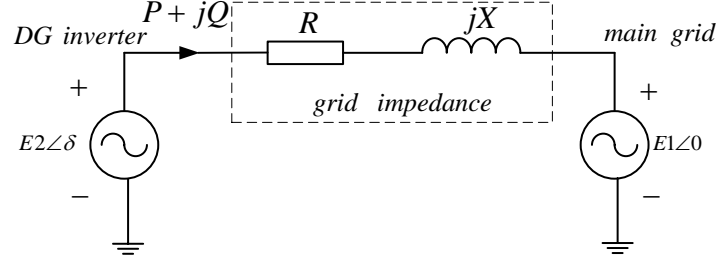

Fig. 2 Equivalent structure of a voltage source inverter (VSI) connected to the common grid.

III.   FUNDAMENTAL IMPEDANCE IDENTIFICATION IN THE GRID-CONNECTED MODE

A. Theoretical analysis of the fundamental impedance identification

Figure 2 shows that when the reactive power is zero, Equation (4) yields

$$E_1(E_1 - E_2\cos\delta) = RP. \tag{5}$$

Suppose that the power angle δ is small, we can assume that $\sin\delta \approx \delta$ and $\cos\delta \approx 1$. Therefore, we can derive the following equation:

$$E_1(E_1 - E_2) \cong RP. \tag{6}$$

Equation (6) is equivalent to

$$R \cong E_1 \frac{E_1 - E_2}{P}. \tag{7}$$

The VSI output power is expressed as $\Delta E = E_1 - E_2$

$$S = P + jQ = P = E_1 I \cos\varphi = E_1 I = E_1 \frac{\Delta E}{Z} = E_1 \frac{E_1 - E_2}{Z}, \tag{8}$$

where φ is the phase angle between the voltage and current. If $\varphi = 0$, then E_1 and E_2 will have the same phase. Subsequently, we can obtain the following:

$$Z = E_1 \frac{E_1 - E_2}{P}. \tag{9}$$

Combining Equations (7) and (9) results in $Z = R$. In this case, only the effect of fundamental resistance on power should be considered. The effect of fundamental inductive reactance on power can be neglected. Consequently, the

effect of line fundamental resistance on power can be estimated when $Q = 0$. The estimated value is not influenced by the reactance.

Figure 2 shows that when the active power is set to zero, we can obtain the following formula by integrating Equation (4):

$$E_1(E_1 - E_2\cos\delta) \cong XQ. \tag{10}$$

When $\sin\delta \cong \delta$ and $\cos\delta \cong 1$, we can obtain

$$E_1(E_1 - E_2) \cong XQ. \tag{11}$$

Equation (11) can be rewritten as

$$X = E_1\frac{E_1 - E_2}{Q}. \tag{12}$$

Similarly, the VSI output power is given by

$$S = P + jQ = jQ = jE_1I\sin\varphi = jE_1I = jE_1\frac{\Delta E}{Z} = jE_1\frac{E_1 - E_2}{Z}, \tag{13}$$

where $\varphi = 90^\circ$; thus, the following expression can be obtained:

$$Z = E_1\frac{E_1 - E_2}{Q}. \tag{14}$$

Combining Equations (12) and (14) results in $Z = X$. In this case, only the fundamental inductive reactance affects the system, whereas the fundamental resistance does not affect the system. Therefore, the line fundamental inductive reactance can be estimated when the system has no active power flow, and the estimated value is not influenced by the resistance of the line impedance.

B. Realization of the fundamental impedance identification

When the constant power control approach is adopted, we maintain the reactive power at zero and vary the active power from $P^*/2$ to P^* to obtain fundamental resistance in the grid-connected mode at the fundamental frequency, i.e., no reactive power flow occurs between the microgrid and main grid. Thus, only the active power exists. Fundamental resistance is calculated according to the corresponding values of the inverter output voltage and current vectors under the varying active power condition. To obtain the fundamental inductive impedance, we maintain the active power at zero and vary the reactive power from $Q^*/2$ to Q^* at the fundamental frequency. Thus, no active power flow is transmitted between the microgrid and main grid, and only the reactive power exists. Subsequently, the fundamental inductive reactance is computed according to the homologous values of the inverter output voltage and

current vectors in the varying reactive power condition. The detection of the fundamental impedance works only at the initial phase, whereas the constant active and reactive power (P^*, Q^*) works under normal conditions.

Calculating the voltage and current vectors in the three-phase circuit is difficult. Therefore, the calculation is executed in a dq synchronous coordinate frame by using Equations (15)–(17). Figure 3 shows the block diagram of the fundamental impedance estimation.

$$R = \left| \frac{\overrightarrow{E_{1R}} - \overrightarrow{E_{2R}}}{\overrightarrow{I_{1R}} - \overrightarrow{I_{2R}}} \right| = \sqrt{\frac{(E_{1Rd} - E_{2Rd})^2 + (E_{1Rq} - E_{2Rq})^2}{(I_{1Rd} - I_{2Rd})^2 + (I_{1Rq} - I_{2Rq})^2}} \tag{15}$$

$$X = \left| \frac{\overrightarrow{E_{1X}} - \overrightarrow{E_{2X}}}{\overrightarrow{I_{1X}} - \overrightarrow{I_{2X}}} \right| = \sqrt{\frac{(E_{1Xd} - E_{2Xd})^2 + (E_{1Xq} - E_{2Xq})^2}{(I_{1Xd} - I_{2Xd})^2 + (I_{1Xq} - I_{2Xq})^2}} \tag{16}$$

$$Z = \sqrt{R^2 + X^2} \tag{17}$$

Here, $\overrightarrow{E_{1R}}$, $\overrightarrow{E_{2R}}$ and $\overrightarrow{I_{1R}}$, $\overrightarrow{I_{2R}}$ are the voltage and current vectors, respectively, when $P \neq 0$ and $Q = 0$. Subsequently, the following vectors can be derived:

$$\overrightarrow{E_{1R}} = E_{1Rd} + jE_{1Rq} \tag{18}$$

$$\overrightarrow{E_{2R}} = E_{2Rd} + jE_{2Rq} \tag{19}$$

$$\overrightarrow{I_{1R}} = I_{1Rd} + jI_{1Rq} \tag{20}$$

$$\overrightarrow{I_{2R}} = I_{2Rd} + jI_{2Rq}. \tag{21}$$

Here, $\overrightarrow{E_{1X}}$, $\overrightarrow{E_{2X}}$ and $\overrightarrow{I_{1X}}$, and $\overrightarrow{I_{2X}}$ are the voltage and current vectors, respectively, when $P=0$ and $Q \neq 0$. In this situation, the following equations can be derived:

$$\overrightarrow{E_{1X}} = E_{1Xd} + jE_{1Xq} \tag{22}$$

$$\overrightarrow{E_{2X}} = E_{2Xd} + jE_{2Xq} \tag{23}$$

$$\overrightarrow{I_{1X}} = I_{1Xd} + jI_{1Xq} \tag{24}$$

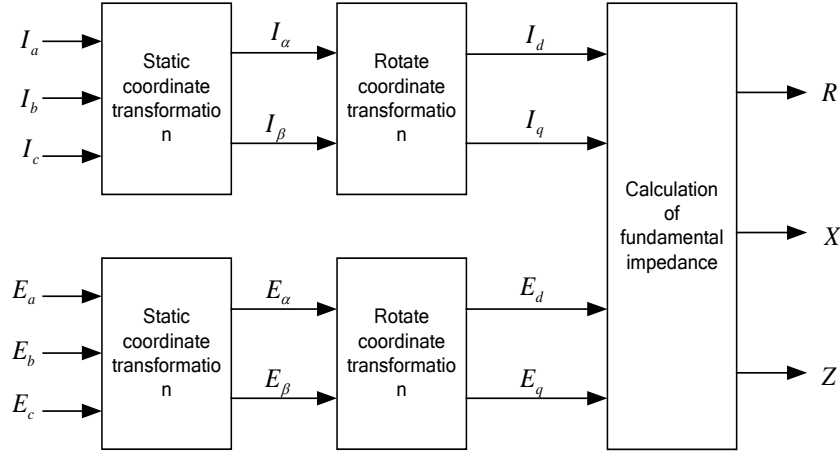$$\overrightarrow{I_{2X}} = I_{2Xd} + jI_{2Xq}. \tag{25}$$

Fig. 3 Implementation block diagram.

IV.   SIMULATION RESULTS

A. Simulation parameters

The proposed control was tested by simulation to validate its feasibility. The simulations used a microgrid consisting of a two-DG system (see Figure 1). The system parameters are shown in Table I.

TABLE I SIMULATION SYSTEM PARAMETERS

Parameter	Values
Rated power	10kW+j2kvar
Load power	30kW+j7.5kvar
DG1 line impedance	0.5Ω+j0.064684 Ω
DG2 line impedance	0.7Ω+j0.064684 Ω
Maximum power	20 kW+j4 kvar

B. Simulation waveforms

Figure 4 shows the variation in the given power in the grid-connected mode under constant power. The active power varied from 5 kW to 10 kW, whereas the reactive power was maintained at zero before t=2 s. To obtain the value of the fundamental resistance, two steady-state voltage and current values were collected during the change in active power. After t=2 s, the reactive power varied from 1 kvar to 2 kvar, whereas the active power was maintained at zero. In this case, the value of the fundamental inductive reactance was obtained by capturing the two steady-state voltage and current values when the reactive power varied.
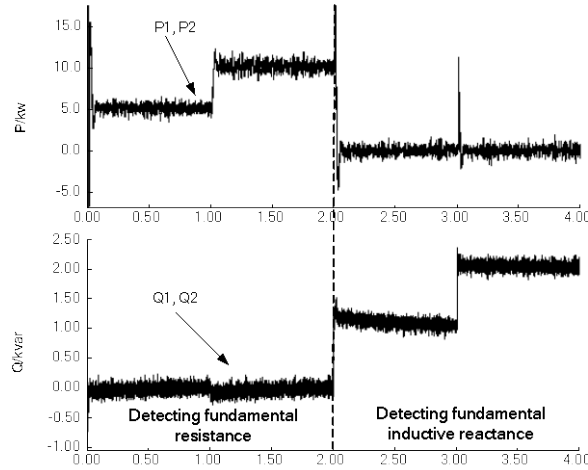
Fig. 4 Output of the (top) active power and (bottom) reactive power by using constant power control in the grid-connected mode.

Figure 5 shows the estimated values of the fundamental impedance in the grid-connected mode. The given simulation parameters and the fundamental impedance simulation results are shown in Table II. From the comparative analysis of the given parameters and the estimated values, the following conclusions can be drawn: the accuracy of the fundamental resistance detection was 98% for DG1, the fundamental reactance detection accuracy was 87% for DG1, the fundamental resistance detection accuracy was 98.4% for DG2, and the fundamental inductive reactance detection accuracy was 93.3% for DG2. The simulation result was consistent with that of the theoretical analysis.
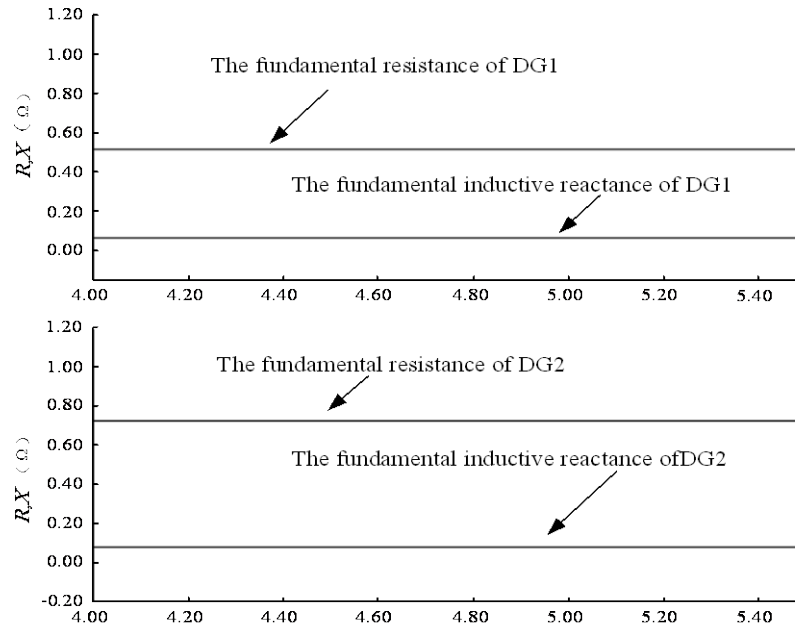

Fig. 5 Detection values of the fundamental resistance and fundamental inductive reactance of (top) DG1 and (bottom) DG2 in the grid-connected mode.

TABLE II FUNDAMENTAL IMPEDANCE PARAMETERS OF THE SPECIFIED AND IDENTIFIED VALUES IN THE SIMULATION

Parameter	Fundamental resistance (Ω)	Fundamental inductive (Ω)
Given value of	0.5	j0.064684
Detected value of	0.510	j0.0558
Given value of	0.7	j0.064684
Detected value of	0.711	j0.0690

The main sources of errors are as follows: 1) current ripples, fluctuation of inverter output current and voltage due to power coupling; 2) A/D sampling; and 3) $\sin\delta \approx \delta$ and $\cos\delta \approx 1$. $\sin\delta \approx \delta$ and $\cos\delta \approx 1$, which are assumptions for Equations (15) and (16), affect the simulation and experiment accuracy. The assumption relationship and evaluation accuracy are related to the active power and reactive power steps. The determination of the power steps variable is a trade-off for the approximate relationship and measurement error of the current and voltage.

V.   EXPERIMENTAL RESULTS

Experiments were performed to show the feasibility of the proposed controller. A three-phase inverter unit was built and tested, and the control was implemented by using a TMS320F2812 DSP. The inverter was connected through a bypass switch to the grid with an equivalent resistance of 5.28 Ω and an inductance of 11.85 mH. The inverter connects to the 380 V grid through a transformer.

A. Experiment for the fundamental resistance estimation

In the grid-connected mode, to evaluate the fundamental resistance, we varied the active power from 20 W to 40 W and maintained the reactive power at zero by using the constant power control method. The fundamental resistance value was then calculated by using Equation (15).

Figure 6 shows the experimental waveform of the inverter's output voltage and current when no reactive power was injected to the grid. The phase of voltage and current is the same, which indicates that only fundamental resistance has an effect on the system.
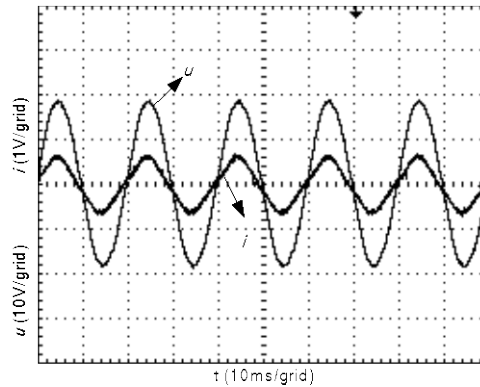

Fig. 6 Voltage and current waveforms when the active power is 20 W and the reactive power is 0 var.

Figure 7 shows the d- and q-axis variations of the inverter's output voltage and current that were detected by DSP. The data of the DSP controller online detection are shown in Table III. The value of the fundamental resistance was obtained by using Equation (26). In particular, the sampling rates of the Hall sensor and A/D sampling were 18.61 and 218.4, respectively.

$$R = \sqrt{\frac{(u_{d1} - u_{d2})^2 + (u_{q1} - u_{q2})^2}{(i_{d1} - i_{d2})^2 + (i_{q1} - i_{q2})^2}} = \sqrt{\frac{(\frac{-28-9}{18.61})^2 + (\frac{400-368}{18.61})^2}{(\frac{-15-2}{218.4})^2 + (\frac{273-148}{218.4})^2}} = 4.5508\Omega \tag{26}$$

The actual line fundamental resistance in the experiment was 5.28 Ω, whereas the detected fundamental resistance was 4.5 Ω, resulting in an accuracy of 85.5%.
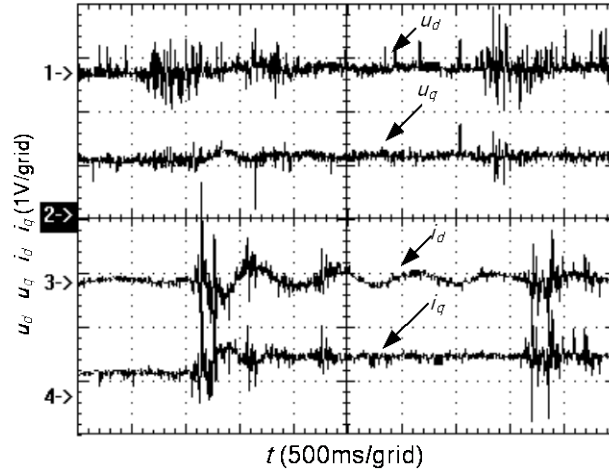

Fig. 7 Variations in u_d, u_q, i_d, and i_q when the active power varies from 20 W to 40 W and the reactive power is 0 var.

TABLE III ONLINE MEASUREMENT RESULTS WHEN THE REACTIVE POWER IS 0 VAR AND THE ACTIVE POWER VARIES

P	Q	u_d	u_a	i_d	i_a
20 W	0 var	−28 V	368 V	−15 A	148 A
40 W	0 var	9 V	400 V	2 A	273 A

B. *Experiment for the fundamental inductive reactance estimation*

In the grid-connected mode, to detect the fundamental inductive reactance, we changed the reactive power from 20 W to 40 W and maintained the active power at zero. The fundamental inductive reactance was calculated by using Equation (16).

Figure 8 shows the experimental waveforms of the inverter output voltage and current when no active power was injected into the microgrid system; the phase difference of the voltage and current is 90°. This finding indicates that only the fundamental inductive reactance had an effect on the system.
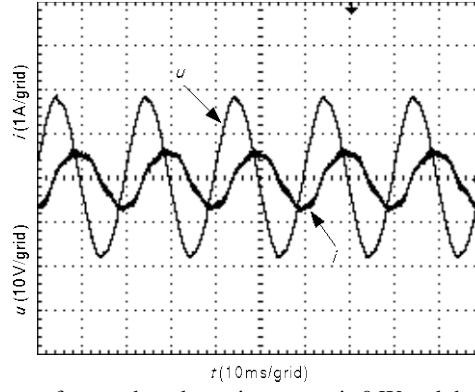
Fig. 8 Voltage and current waveforms when the active power is 0 W and the reactive power is 20 var.

Figure 9 shows the d- and q-axis variations of the inverter's output voltage and current. The online detection employed was based on the DSP controller. The data are shown in Table IV. The value of the fundamental inductive reactance was calculated by using Equation (27).

$$R_{\mathrm{L}} = \sqrt{\frac{(u_{\mathrm{d1}} - u_{\mathrm{d2}})^2 + (u_{\mathrm{q1}} - u_{\mathrm{q2}})^2}{(i_{\mathrm{d1}} - i_{\mathrm{d2}})^2 + (i_{\mathrm{q1}} - i_{\mathrm{q2}})^2}} = \sqrt{\frac{(\frac{-110+150}{18.61})^2 + (\frac{344-344}{18.61})^2}{(\frac{-157+275}{218.4})^2 + (\frac{-50+120}{218.4})^2}} = 3.42145\Omega \tag{27}$$

$$L = \frac{R_{\mathrm{L}}}{2\pi f} = 10.896\mathrm{mH} \tag{28}$$

The actual line fundamental inductance in the experiment is 11.85 mH, whereas the detected fundamental inductance is 10.896 mH, resulting in a 91.9% accuracy.
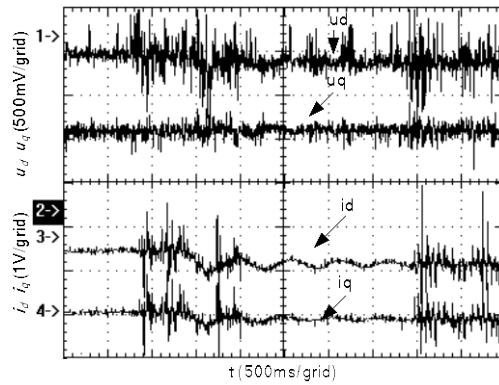

Fig. 9 Variation in ud, uq, id, and iq when the active power is 0 W and the reactive power varies from 20 var to 40 var.

TABLE IV ONLINE MEASUREMENT RESULTS WHEN THE ACTIVE POWER IS 0 W AND THE REACTIVE POWER VARIES

P	Q	u_d	u_q	i_d	i_q
0W	20var	−110V	344V	−157A	−50A
0W	40var	−150V	344V	−275A	−120A

VI. CONCLUSION

Considering the importance of line fundamental impedance in the microgrid system, this paper presented a novel fundamental impedance identification strategy by varying the operating power in the grid-connected mode. Theoretical analysis and formula derivation of the fundamental impedance were performed, and the implementation flowchart under varying output power reference was presented. The identification method was simple and easy to implement, and the real-time online identification progress yielded an accurate evaluation.

ACKNOWLEDGMENT

REFERENCES

[1] Min Dai, Mohammad N.Marwali, Jin-Woo Jung, Ali Keyhani.: 'Power flow control of a single distributed generation unit with nonlinear local load'. Power Systems Conf. And Exposition IEEE/PES, 10-13 Oct 2004, pp. 398-403

[2] Emanuel Serban, Helmine Serban.: 'A control strategy for a distributed power generation microgrid application with voltage and current controlled source converter'. *IEEE Trans. Power Electr.*, 2010,**25**, (12), pp. 2981-2992

[3] Josep M. Guerrero, Luis Garcia de Vicuna, Jose Matas, Miguel Castilla, Jaume Miret.:'A wireless controller to enhance dynamic performance of parallel inverters in distributed generation system'. *IEEE Trans. Power Electr.*, 2004 ,**19**,(5), pp. 1205-1213

[4] F.Blaabjery, Z.Chen, S.B.Kjaer.: 'Power electronics as efficient interface in dispersed power generation systems'. *IEEE Trans. Power Electr.*, 2004, **19**, (5), pp. 1184-1194

[5] R.Lasseter. Microgrid. IEEE Power Eng. Soc, pp. 305-308, 2002.

[6] Yunwei Li, Ching-Nan Kao.: 'An accurate power control strategy for power-electronics-interfaced distributed generation units operating in a low-voltage multibus microgrid'. *IEEE Trans. Power Electr.*, 2009, **24**, (12), pp. 2977-2988

[7] N.Pogaku, N.Prodanovic, T.C.Green.: 'Modeling, analysis and testing of autonomous operation of an inverter-based microgrid'. *IEEE Trans. Power Electr.*, 2007,**22**, (2), pp. 613-625

[8] A.Hasanzadeh, O.C.Onar, H.Mokhtari, A.Khaligh.: 'A proportional –resonant controller-based wireless control strategy with a reduced number of sensors for parallel-operation UPSs'. *IEEE Trans. Power Deliv.*, 2010, **25**, (1), pp. 468-478

[9] Y. Li, and Y. W. Li.: 'Power management of inverter interfaced autonomous microgrid based on virtual frequency-voltage frame'. *IEEE Trans. Smart grid.*, 2011,**2**,(1), pp. 30-40

[10] Y. Mohamed and E.Saadany.: 'Adaptive decentralized droop controller to preserve power sharing stability of parallel inverters in distributed generation microgrids'. *IEEE Trans. Power Electr.*, 2008,**23**,(6), pp. 2806-2816

[11] D.N.Zmood, D.G.Holmes, G.H.Bode.: 'Stationary frame current regulation of PWM inverters with zero steady-state error'. *IEEE Trans. Power Electr.*, 2003, **18**, (3), pp. 814-822

[12] F.Katiraei, M.R.Iravani.: 'Power management strategies for a microgrid with multiple distributed generation units'. *IEEE Trans . Power Syst.*, 2006, **21**, (4), pp. 1821 -1831

[13] Y.W.Li, D.M.Vilathgamuwa, P.C.Loh.:'Design, analysis and real-time testing of controllers for multi-bus microgrid system'. *IEEE Trans. Power Electr.*, 2004, **19**, (5), pp. 1195 -1204

[14] J.M.Guerrero, J.Matas, L.G.Vicuna, M.Castilla, J.Miret.: 'Decentralized control for parallel operation of distributed generation inverters using resistive output impedance' . *IEEE Trans. Ind. Electr.*, 2007, **52,** (4), pp. 994 -1004

[15] J.M.Guerrero, J.Matas, L.G.Vicuna, M.Castilla, J.Miret.: 'A wireless controller to enhance dynamic performance of parallel inverters in distributed generation systems' . *IEEE Trans. Ind. Electr.*, 2004, **19**, (5), pp. 1205 -1213

[16] J.M.Guerrero, J.Matas, L.G.Vicuna, M.Castilla, J.Miret.: 'Output impedance design of parallel-connected UPS inverters with wireless load-sharing control' . *IEEE Trans. Ind Electr.*, 2005vol. **52**, (4), pp. 1126 -1135

[17] Karel De Brabandere, Bruno Bolsens, Jeroen Van den Keybus, Achim Woyte, Ronnie Belmans.: 'A voltage and frequency droop control method for parallel inverters'. *IEEE Trans. Power Electr.*, 2009, **24**, (12), pp. 2977-2988

[18] Yan Li, Yun Wei Li.: 'Virtual frequency –voltage frame control of inverter based low voltage microgrid.' IEEE Electrical Power& Energy Conf.(EPEC'09), 22-23 Oct 2009, pp. 1-6

[19] A.Tuladhar, H.Jin, T.Unger, K.Mauch.: 'Parallel operation of single phase inverter modules with no control interconnections' . Twelfth Annual Applied Power Electronics Conf. And Exposition (APEC'97), Atlanta, GA, 1997, pp. 94-100

[20] A.V. Timbus, P. Rodriguez, R. Teodorescu, M. Ciobotaru.: 'Line Impedance Estimation Using Active and Reactive Power Variations'. IEEE Power Electronics Specialists Conf.(PESC'07), 17-21 June 2007, pp. 1273 -1279

[21] J.C. Vasquez, J.M. Guerrero, A. Luna, P. Rodriguez, R. Teodorescu.: 'Adaptive droop control applied to voltage-source inverters operating in grid-connected and islanded modes'. *IEEE Trans. Ind Electr.*, 2009, **56**, (10), pp. 4088-4096

[22] L. Asiminoaei, R. Teodorescu, F. Blaabjerg, and U. Borup.: 'A digital controlled PV-inverter with grid impedance estimation for ENS detection'. *IEEE Trans. Power Electr.*, 2005, **20**, (6), pp. 1480-1490

[23] M. Liserre, R. Teodorescu, and F. Blaabjerg.: 'Stability of photovoltaic and wind turbine grid-connected inverters for large set of grid impedance values'. *IEEE Trans. Power Electr.*, 2006, **21**, (1), pp. 263-272

[24] J Huang, K.A. Corzine, M. Belkhayat.: 'Small-signal impedance measurement of power-electronics-based AC power systems using line-to-line current injection'. *IEEE Trans. Power Electr.*, 2009, **24**, (2), pp. 445-455